

# The Effect of the Third Element on Corrosion Behavior and Phase Structure of Fe35Mn Alloy Fabricated by Spark Plasma Sintering (SPS)

Nahid Hassanzadeh Nematia<sup>1\*</sup>, Mahdis Parsafar<sup>1</sup>

<sup>1</sup>Department of Biomedical Engineering, Science and Research Branch, Islamic Azad University, Tehran, Iran

\*Email of Corresponding Author: nahid\_hassanzadeh@yahoo.com; hasanzadeh@srbiau.ac.ir

Received: August 3, 2019; Accepted: November 11, 2019

## Abstract

In recent years, investigations on accelerating of corrosion of Fe-Mn based alloys as biodegradable ones in orthopedic applications are aggrandized. Alloy composition is one of the effective factors in this case. This study is focused on the effect of the third element on the corrosion behavior of Fe35Mn alloy. For this purpose, four alloys including Fe35Mn, Fe35Mn2Ti, Fe35Mn2Ta, and Fe35Mn2Zr were produced by mechanical alloying. Then cylindrical samples of each alloy were fabricated by spark plasma sintering method (SPS) with pressing in 50MPa and sintering at 1000°C for 20 minutes simultaneously. All the specimens were evaluated by x-ray diffraction (XRD), light microscope, and potentiodynamic polarization test to compare the effect of the third element as Ta, Ti, and Zr. Results revealed that adding the third element increases the corrosion rate. It is found that the most effective element was Ta. Also, the weight changes of specimens after immersion in SBF at different times for predicting their probable behavior in the human body were measured. The findings could be utilized in medical applications.

## Keywords

Degradable Alloy, Microstructure, Electrochemical Measurements, Spark Plasma Sintering

## 1. Introduction

Biodegradable metals are materials that corrode gradually in vivo with no toxic residues. So, they have no undesirable effect from corrosion products to the surrounded host tissue, while the problem with other alloys is their corrosion behavior as their residues are toxic. Till now, biodegradable metals have been categorized into three main systems: Fe, Mg, and Zn based alloys [1]. Among them, Fe based biodegradable metals are more attractive because of their suitable strength, good ductility [2], corrosion rate, and no hydrogen release which results in pain and inflammation in host tissue [3]. They also have higher strength and younger modulus than Mg-based alloys [4]. Other Researches on Fe-Mn [5- 7] found out their shape memory effect and intelligent behavior.

Adding a third element to Fe-Mn binary alloys can make significant changes in their mechanical and corrosion properties. The effect of Si in the mentioned properties of the alloy was studied before as a third element [3, 5, 6, 8, 9]. Also, Ag adding to this alloy for being as an antibacterial alloy has been studied before [10]. But the effects of Ti, Zr, and Ta as biocompatible metals on characteristics of Fe-Mn alloys have not been investigated yet. So that was noticed in this research after three compositions including Fe-Mn-Zr, Fe-Mn-Ti, and Fe-Mn-Ta were fabricated by mechanical alloying and then spark plasma sintering (SPS).

SPS is an appropriate processing technique for fabricating metallic devices. It has many benefits such as decreasing work time, improving density, and enhancing the mechanical properties of samples [11].

In the end, as the novelty of the paper is adding the third element of Ta, Ti, and Zr and studying their effects on Fe35Mn on its corrosion behavior, by evaluating and concluding the best third element, that alloy could be operative in medical applications as a biodegradable implant in orthopedic surgeries.

## 2. Materials and Method

Powders used in this study were Fe, Ti, and Zr with 99.9% purity (MERC, particle size  $<63 \mu\text{m}$ ). The powders were dry milled in Retsch planetary mill for 2 h, at a rotation speed of 275 rpm and a ball-to-powder weight ratio of 5:1 (the balls were made of steel with the diameter of 8mm) for obtaining Fe-35Mn-2Ti, Fe-35Mn-2Zr, and Fe-35Mn-2Ta (%wt) compositions. These as-milled powders were sintered in SPS (Easy fashion 20T-10) at  $1000^\circ\text{C}$  temperature under 50MPa and vacuum pressure of  $10^{-4}$  torr for 20 minutes. The as-sintered cylindrical alloys have been wire cut for  $10 \times 10$  mm pieces.

Phase structures of mechanically alloyed powders were evaluated by XRD (Seisert PTS3003) with radiation of  $\text{CuK}\alpha$  and  $\lambda=1.54\text{\AA}$ . The corrosion behavior of the spark plasma sintered specimens were studied by potentiodynamic polarization test (Potentiostat EG&G 273A) in the potential window of -1600 mV to 1000 mV below the open circuit potential (OCP) and with scanning rate of 0.65 mV/S after immersion in HANKS [12] solution ( $37^\circ\text{C}$  and  $\text{pH} = 6.8$ ). In this test, a three-electrode cell was applied in which Platinum is applied as the counter electrode, saturated calomel as a reference electrode, and the sample as a working electrode. The obtained data were analyzed by the review software.

The surface morphology of all specimens was observed using an optical microscope (Olympus BX51M) after spending metallographic stages. The porosity of samples was measured by Olysia software and microscope (Olympus DP12CK40M). Also, the changes in the weight of the alloy were obtained in 1 month (at different periods) by immersing samples in SBF in the temperature of  $37^\circ\text{C}$  while samples were incubated in an orbital incubator. Then pH changes after immersion of each alloy were observed by Crison pH meter and light microscopic images of samples were taken while immersion.

## 3. Results and Discussion

The XRD spectra of alloys powder after mechanical alloying is presented in Figure 1. The defined peaks at  $2\theta$  of about 44 and 51 degrees relate to austenite structure [3, 6, 13], around 43 and 82 represented martensite structure and 65 refers to the ferrite phase [6, 14, 15]. As it is obvious in Figure 1, austenite and martensite phase exist in all three alloys with a third element. The existence of austenite in the experimental condition temperature of  $25^\circ\text{C}$  indicates that the alloying procedure occurred truly because Mn joined Fe structure and therefore stabilized austenite phase [16]. The presence of Martensite in spectra relate to striking of metal powders and balls in mechanical alloying and performing stress-induced martensite. As Mn is austenite phase stabilizer and its weight percent is 35 in all alloys, the obtained results were predictable. Zirconium, tantalum, and

titanium are ferrite phase stabilizers but the presence of Mn in high percentage overcomes and only a weak peak in  $65^\circ$  can be observed in XRD spectra of Fe-35Mn-2Ti, Fe-35Mn-2Zr, and Fe-35Mn-2Ta alloys. It relates to the presence of the mentioned elements in the compositions or insufficient alloying but non-appearance of  $65^\circ$  peak in Fe-Mn alloy proves the first theory relevant to adding the third element.

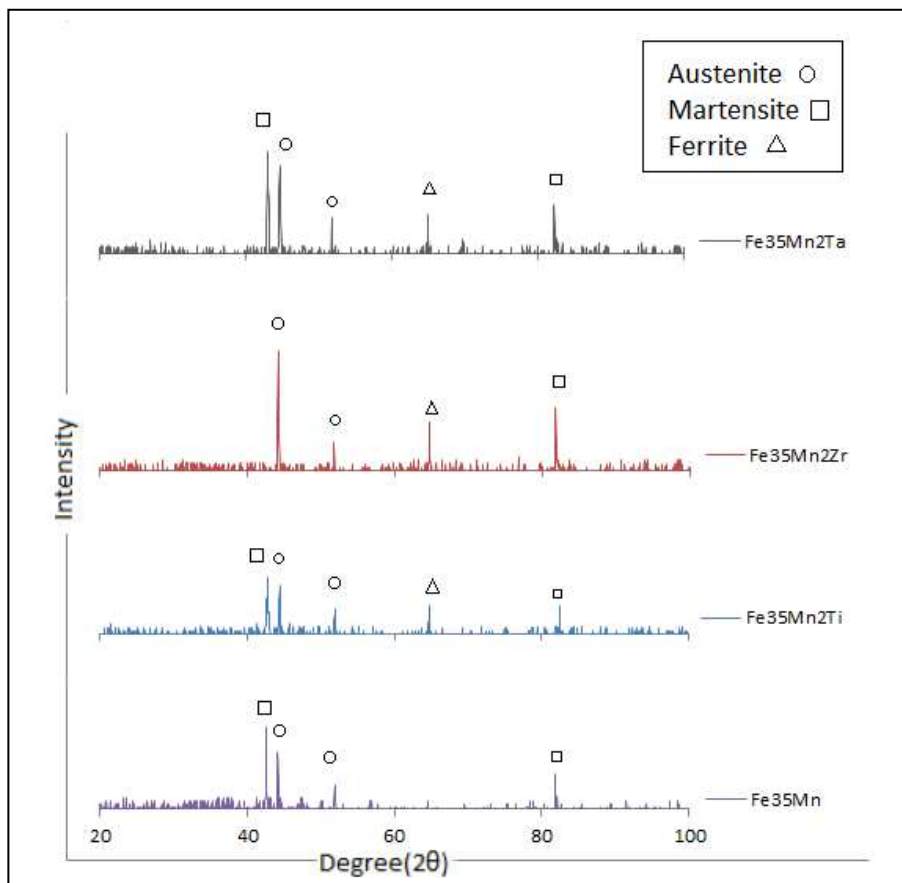


Figure1. XRD spectra of mechanical alloyed Fe-Mn, Fe-Mn-Ti, Fe-Mn-Ta, and Fe-Mn-Zr powders

The results of the potentiodynamic polarization test are shown in Figure 2. Corrosion current density and corrosion potential are given in Table 1. By comparing these values, the increase in corrosion by adding the mentioned third elements to Fe-Mn alloy is obvious. The most corrosion current density relates to Fe-Mn-Ta and the least corrosion belongs to Fe-Mn-Zr. Ti, Ta, and Zr is Ferrite phase stabilizers that the related peak can be observed in Figure 1. On the other hand, the existence of the third element increases the probability of corrosion by producing various precipitations and therefore accelerates corrosion.

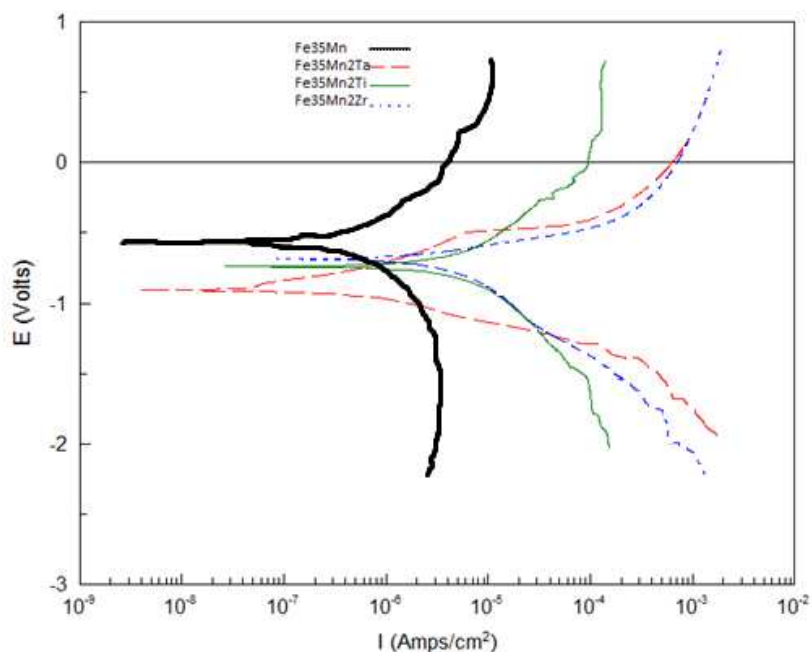


Figure2. Potentiodynamic polarization curves of Fe-Mn, Fe-Mn-Ti, Fe-Mn-Ta, and Fe-Mn-Zr samples

According to Table1, the corrosion resistance ( $R_p$ ) of the alloys from the most to the least can be presented in the following pattern:

Fe-Mn > Fe-Mn-Zr > Fe-Mn-Ti > Fe-Mn-Ta

The Fe-Mn alloy fabricated by 3D printing and conventional powder metallurgy at the same conditions with ours has lower corrosion potential [1, 17]. It indicates that by SPS fabrication method that pressure and temperature are applied together to the sample, the corrosion potential increases and is about -0.6 V. which can be the result of its porosity reduction property.

Table1. Corrosion parameters of alloys fabricated by SPS

Alloy	Corrosion Current Density ( $\mu\text{A}/\text{cm}^2$ )	Corrosion Potential (V)	$R_p$ (ohm/cm <sup>2</sup> )
Fe35Mn	12.745	-0.56929	1924
Fe35Mn2Ta	21.408	-0.90513	1677
Fe35Mn2Ti	19.739	-0.73938	1701
Fe35Mn2Zr	16.608	-0.68699	1749

Optical micrographs (Figure 3) show that all of the alloys are nearly dense with low porosity that relates to the fabrication method (SPS). There are at least two separate phases in microstructures. The mother phase which is illustrated with bright color is austenite. Mn stabilizes the FCC structure of Fe at room temperature. The presence of the second phase is more in alloys with the third element. It could be a reason for their less corrosion resistance than Fe35Mn. By analyzing data taken by Olysia software (Table 2), one could conclude that adding the third element increases the percentages of pores.

Increasing corrosion density of the alloy without the third element from 12.74 to 21.41, 19.74 and 16.61  $\mu\text{A}/\text{cm}^2$  for the alloy including Ta, Ti, and Zr, respectively approved the formation of more

micro electrochemical cells in them. The more phase segregation at grain boundaries in the alloys with the third element is another conclusion.

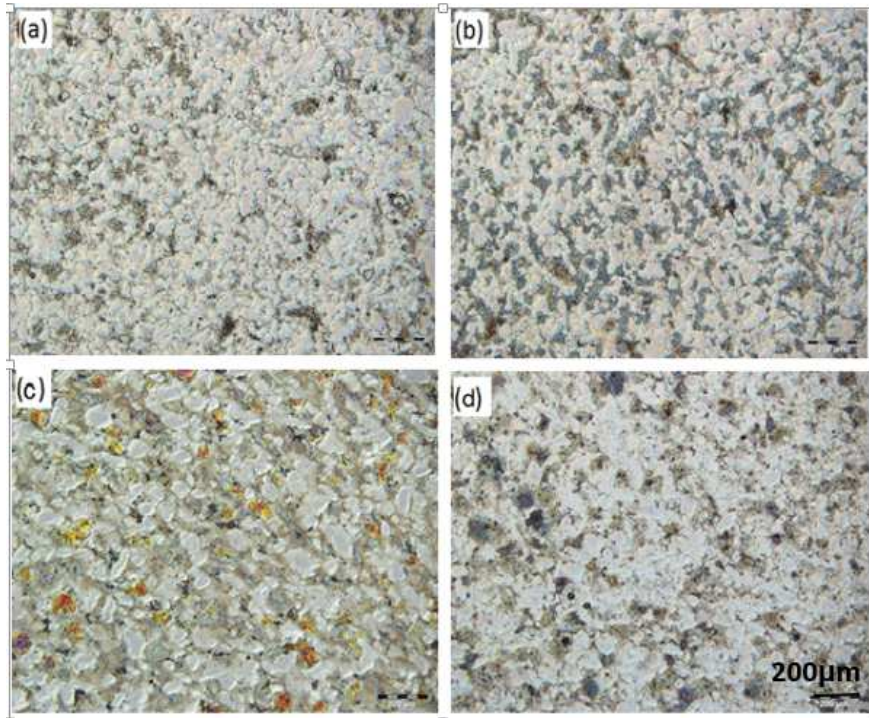


Figure3. Optical microscopic Images of (a): Fe35Mn2Zr, (b): Fe35Mn2Ti, (c): Fe35Mn2Ta, (d): Fe35Mn

Table2. The porosity of Fe35Mn2Ti and Fe35Mn2Zr

Alloy	Porosity%
Fe35Mn	1.43
Fe35Mn2Zr	4.01
Fe35Mn2Ta	7.87
Fe35Mn2Ti	4.64

Weight measurements of the alloys after drying follow to immersion in different periods in SBF are shown in Figure 4. The results show that the weight of Fe35Mn, Fe35Mn2Zr, and Fe35Mn2Ti augments with increasing the time of immersion because of the deposition layer increasing. It is expected that by depositing the calcium phosphate salt in the solution on the alloy, the weight augments. It also shows that the precipitation rate is more quickly than the degradation rate but for Fe35Mn2Ta alloy it was different and we observed weight loss which relates to the rapid corrodible nature of Ta. According to the results of the previous tests, the most corrosion rate relates to this alloy. So it can be concluded that because of the significant reduction effect of Ta on corrosion resistance of Fe35Mn, there is no chance for layer precipitation or if the deposition happened, the high rate of degradation overcomes the weight increase. But after 14 days, the precipitate was so high that it defeated weight loss due to corrosion.

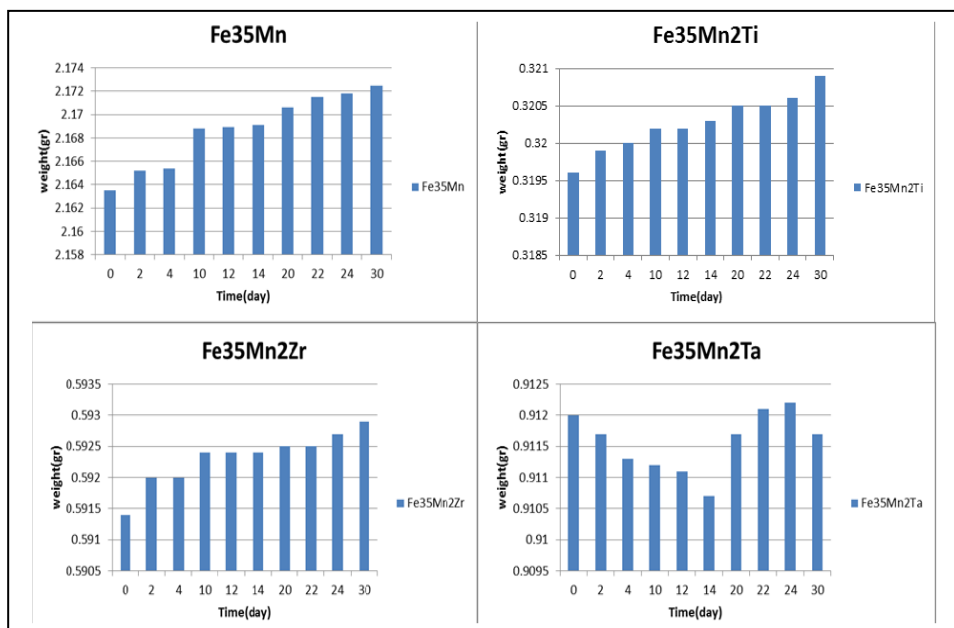


Figure4. Changes in the weight of alloys of Fe35Mn, Fe35Mn2Ti, Fe35Mn2Zr, and Fe35Mn2Ta in different immersion times

After immersion, pH of the solution changes depending on the alloy and it was observed that all solutions become alkaline which the most effect relates to Fe35Mn. It means that adding the third element affects the acidity of its environment (Table 3). Surface samples indicate high levels of corrosion in a short time after immersion in SBF. The light microscopic images of samples after 10 and 30 days show increasing degradation (Figure 5).

Table3. Solution pH after immersion of each alloy

Alloy	pH
Control	6.8
Fe35Mn	9.36
Fe35Mn2Ti	8.56
Fe35Mn2Ta	8.32
Fe35Mn2Zr	8.38

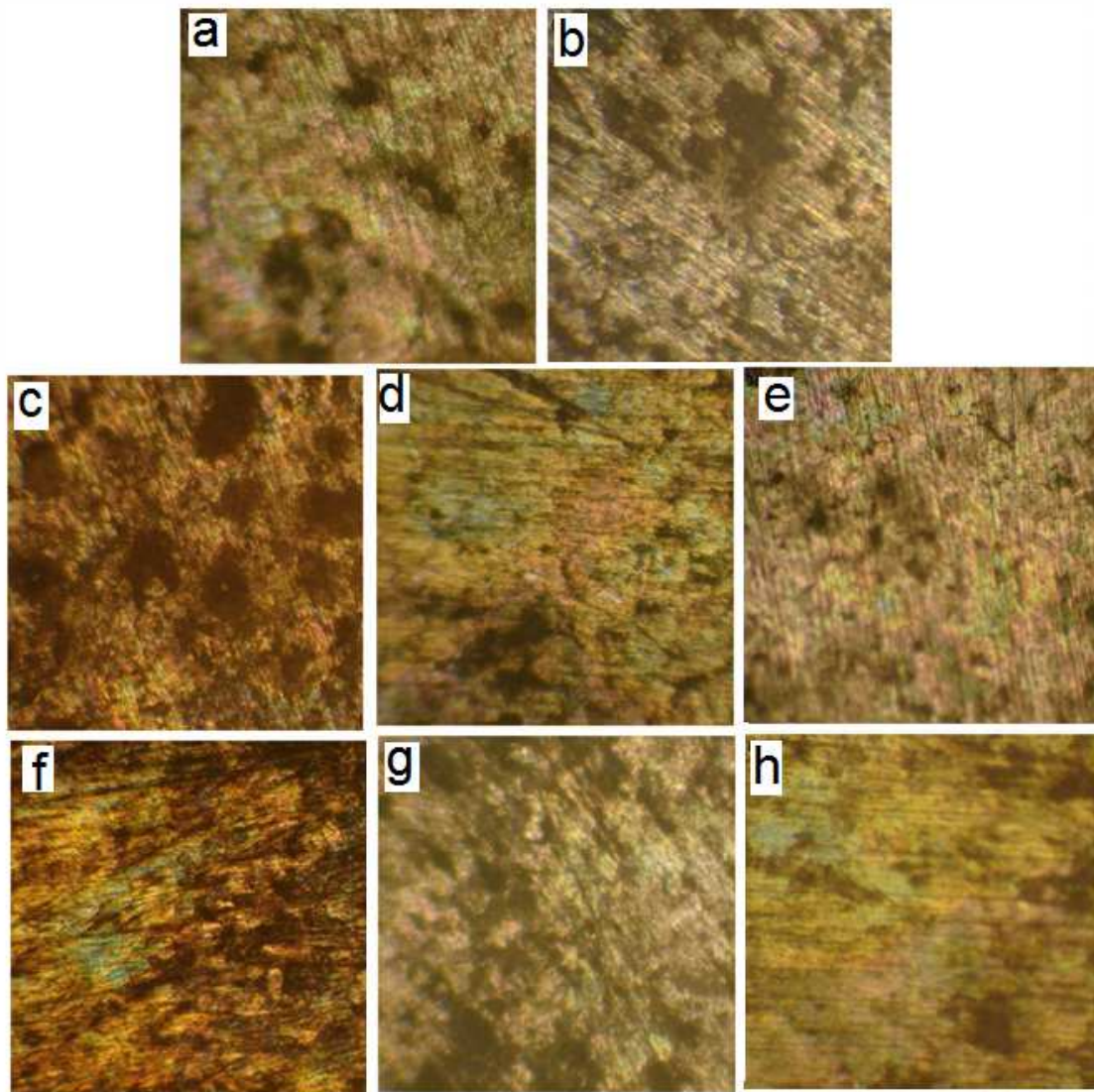


Figure5. Light microscopic images of (a,b)Fe35Mn after 10 and 30 days respectively. (c,f) Fe35Mn2Ta after 10 and 30 days, (d,g) Fe35Mn2Ti after 10 and 30 days and (e,h) Fe35Mn2Zr after 10 and 30 days (Magnification: 100x)

#### 4. Conclusion

In this paper, the effect of Ti, Ta, and Zr as the third element to Fe35Mn alloy fabricated by SPS was studied and the following points are given:

The observation of austenite phase in Fe35Mn alloy in experimental conditions, such as the temperature of 25°C, demonstrates that the alloying was accomplished properly. The ferrite phase discovered in Fe35Mn2Ti, Fe35Mn2Zr, and Fe35Mn2Ta indicates that these third elements are ferrite phase stabilizers.

1. Martensite structure observed in all four alloys relates to mechanical alloying stresses which result in induced Martensite structures.
2. The potentiodynamic polarization test shows that adding all these three elements decreases corrosion resistance because of the presence of more than one-phase in their microstructures. Ta and Zr have the most and the least effect respectively.

3. Optical microscopic images illustrated a good density in all of the alloys related to the SPS method. The maximum porosity is about 8%, which seems to be lower than traditional powder metallurgy manufacturing methods.
4. As Ta makes more corrosion current density and has the least effect on Ferrite induction, it may be a better candidate among these four alloys after successfully passing the biocompatibility test for biodegradable medical purposes.

## 5. References

- [1] Huafang, L., Yufeng, Z. and Ling, Q. 2014. Progress of Biodegradable Metals. *Materials International*. 24: 414–422.
- [2] Kraus, T., Moszner, F., Fischerauer, S., Fiedler, M., Martinelli, E., Eichler, J., Witte, F., Willbold, E., Schinhammer, M., Meischel, M., Uggowitzner, P., Löffler, J. and Weinberg, A. 2014. Biodegradable Fe-based alloys for use in osteosynthesis: Outcome of an in vivo study after 52 weeks. *Acta Biomaterialia*, 10: 3346–3353.
- [3] Xu, Z., Hodgson, M. and Cao, P. 2015. A comparative study of powder metallurgical (PM) and wrought Fe–Mn–Si alloys. *Materials Science & Engineering A*. 630: 116–124.
- [4] Niinomi, M., Nakai, M. and Hieda, J. 2012. Development of new metallic alloys for biomedical applications. *Japan Acta Biomaterialia*, 8: 3888–3903.
- [5] Zhang, W., Wen, Y., Li, N. and Huang, S. 2007. Remarkable improvement of recovery stress of Fe–Mn–Si shape memory alloy fabricated by equal channel angular pressing, *Materials Science and Engineering*. 454: 19–23.
- [6] Liu, B., Zheng, Y. and Ruan, L. 2011. In vitro investigation of Fe<sub>30</sub>Mn<sub>6</sub>Si shape memory alloy as potential biodegradable metallic material. *Materials Letters*. 65: 540–543.
- [7] Liu, Y., Zhang, X., Xing, D., Shen, H., Chen, D., Liu, J. and Sun, J. 2014. Magnetocaloric effect (MCE) in melt-extracted Ni–Mn–Ga–Fe Heusler microwires. *Journal of Alloys and Compounds*. 616: 184–188.
- [8] Hermawan, H. and Mantovani, D. 2013. Process of prototyping coronary stents from biodegradable Fe–Mn alloys. *Acta Biomaterialia*. 9: 8585–8592.
- [9] Drevet, R., Zhukova, Y., Malikova, P., Dubinskiy, S., Korotitskiy, A., Pustov, Y. and Prokoshkin, Y. 2018. Martensitic Transformations and Mechanical and Corrosion Properties of Fe-Mn-Si Alloys for Biodegradable Medical Implants. *Metallurgical and Materials Transactions A*. 49: 1006–1013.
- [10] Sotoudebagha, P., Sheibani, S., Khakbiz, M., Ebrahimi-Barough, S. and Hermawan, H. 2018. Novel antibacterial biodegradable Fe-Mn-Ag alloys produced by mechanical alloying. *Materials Science and Engineering C*. 88: 88–94.
- [11] Suárez, M., Fernández, A., Menéndez, J., Torrecillas, H., Kessel, J., Hennicke, R., Kirchner, R. and Kessel, T. 2007. Challenges and Opportunities for Spark Plasma Sintering: A Key Technology for a New Generation of Materials. *Material Research Centre*. 10: 319–349.
- [12] Luiz de Assis, S. and Costa, I. 2007. The effect of polarisation on the electrochemical behavior of Ti-13Nb-13Zr alloy. *Material Research Centre*. 10: 293–296.

- [13] Lee, S., Han, J., Lee, C., Park, I. and Lee, Y. 2014. Elastic strain energy induced by epsilon martensitic transformation and its contribution to the stacking-fault energy of austenite in Fe–15Mn–xC alloys. *Journal of Alloys and Compounds*. 617: 588–596.
- [14] Moszner, S., Gerstl, P., Uggowitzer, J. and Löffler, L. 2014. Atomic-scale characterization of prior austenite grain boundaries in Fe–Mn-based maraging steel using site-specific atom probe tomography. *Acta Materialia*. 73: 215–226.
- [15] Aminia, E., Salahinejad, M., Hadianfard, M., Marasi, T. and Sritharan, M. 2010. Characterization of Fe–Cr–Mn–N amorphous powders with a wide supercooled liquid region developed by mechanical alloying. *Materials Science and Engineering A*. 527: 1135–1142.
- [16] Maalekian, M. 2007. The Effects of Alloying Elements on Steels (I). Christian Doppler Laboratory for Early Stages of Precipitation. 14-29.
- [17] Chou, D., Wells, D., Hong, D., Lee, B., Kuhn, H. and Kumta, P. 2013. Novel processing of iron–manganese alloy-based biomaterials by inkjet 3-D printing. *Acta Biomaterialia*. 9:8593–8603.